TECHNISCHE MECHANIK, 32, 2-5, (2012), 265-272
submitted: November 1, 2011

Numerical Evaluation of Compressible Plasticity Behaviour of Metal Foams

S. Imatani

Yielding phenomenon and plastic flow are numerically investigated on a metal foam model from the macroscopic point of view. Based on the computational geometry technique of Voronoi tessellations, closed-cell foam models are constructed with quadrilateral shell elements, and the mechanical responses are evaluated for a relatively small deformation regime by use of the finite element method. The model material reveals compressible plasticity behavior where the normality rule mostly holds. It is also found that material anisotropy is dominant in plate-like materials and bar-like materials, which should be taken into account in the practical utilization.

1 Introduction

Metal foams have specific features of extremely low density, high shock absorption, low thermal conductivity, and so on. These characteristics enable us to achieve significant energy and material consumption savings as well. Furthermore from suppliers' view, it is advantageous to control and adjust these properties subject to the practical demands through the production process. Overall discussions on the manufacturing processes, mechanical properties, and utilization of metal foams can be found in the monograph by Ashby et al. (2000), and we can find macroscopic models from conventional approach, e.g., Deshpande and Fleck (2000), and from the concept of generalized continua, e.g., Dillard et al. (2006).

Since metal foams are composed of cellular members and the porosity typically takes values over 0.9, which means that the solid occupies only 10% of the total volume while the rests are pores, the mechanical behaviour at the macroscopic level is expected to be completely different from that of substantial ingredients, i.e. metals. Typical phenomena are observed during large deformation processes in the ways that a flat non-hardening region, so-called plateau region, appears in the compressive loading, whereas the material goes to failure shortly after the maximal stress in the tensile loading. For the former, it is well known that the flat region is caused by a simultaneous buckling and collapse of cellular members. In contrast, for the latter, a local neck and its subsequent rupture in a particular cell are supposed to be dominant. Due to these mechanisms the metal foams reveal an asymmetric response with respect to tension and compression.

This paper discusses the validity of conventional theory usually adopted in metal plasticity for the porous metals through the numerical analysis study. The computational geometry technique of Voronoi tessellation is applied and closed-cell foam models are constructed. Each cell member is composed of four-node quadrilateral shell elements, originally proposed by Belytschko and Leviathan (1994), and Zhu and Zacharia (1996). Here we examine the elasto-plastic behaviour of the foam-like material model in terms of macroscopic variables. Particularly we discuss the material response in small deformation. It is found that the macroscopic behaviour of the foam is similar to that of a solid at least with respect to the uniaxial stress-strain response in a small deformation regime, whereas some of the members do not contribute to the plastic deformation. We also examine the compressible plastic yield, the material flow after the normality rule, and the material anisotropy, which are essentially important for the constitutive modeling.

2 Mechanical Behaviour of ALPORAS: An Example of Metal Foam

First we show a typical example of mechanical response of metal foams. The tested material is ALPORAS©, an aluminium based metal foam produced by SHINKO Wire Co LTD, which was originally supplied as a sheet with 10mm in thickness. Figure 1 shows surface views of the material. The size of pores is quite large and random; 3 through 6 mm in diameter, which indicates that only two or three cells exist through the thickness direction, and the shape of each cell is also complex. Then size effects, e.g., Diebels and Steeb (2002) and Tekoglu et al.

(2011), may appear in the macroscopic response. We further observe that the thickness of the cell wall has significant variation. It is clear that such irregular size and shape, i.e. the effect of imperfections from the viewpoint of an idealized concept, have a dominant influence of the mechanical response; probably pull down the onset of buckling and necking, and therefore the material may reveal lower strength than expected. However we should also notice that such irregularities may be advantageous in view of energy absorption or other properties.

Figure 2(a) exhibits an example of ALPORAS specimen on the way of a four-point bending test, in which the load level is under the elastic regime. The total span of the beam specimen is taken as 120mm, which is out of scope in the photograph, while the upper pins of 80mm span are loaded downward. The shape of the cross-section of the specimen is set to be a square as 10mm both in the width and the thickness. As is seen from the broken line, the deflection follows an arc curve by Bernoulli-Navier's kinematics of beam theory. It implies that cell walls in the specimen carry the bending moment, although the configuration of each skeletal cell is far different from a beam. This result tells us that it would be possible, in part, to regard the metal foam with such a small amount of cells as a classical continuum, when the real cell size and numbers under consideration are fixed constant. Further observation should be done for the cross sectional view under the bending. Bending moment diagrams are shown in Figure 2(b) where a wide variety in data is observed in the porous test specimens. For example, the elasticity modulus, which can be calculated from the straight lines in the beginning of the diagram, varies from 500 MPa up to 2000 MPa. The solid marks, which indicate the results for solid aluminum specimens with different shape and dimensions from the metal foam, exhibit a clear reappearance. Since a few number of cells are involved in each specimen, the strength is governed by the weakest cell. This kind of poor ductility is one of the characteristics of a metal foam.

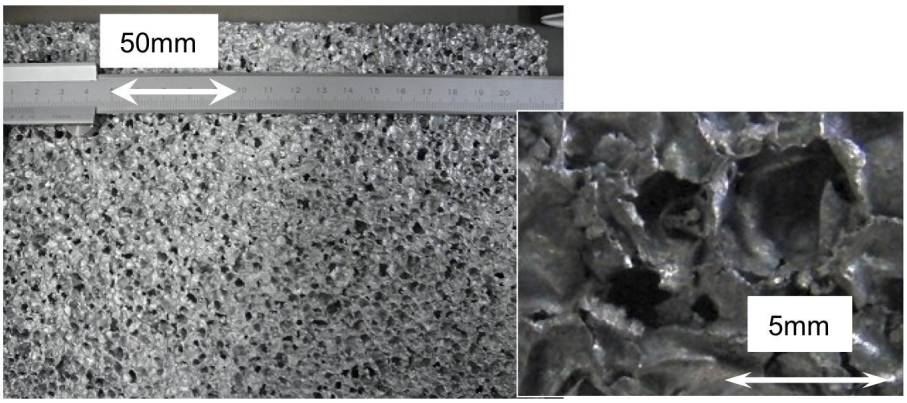

Figure 1. Surface view of metal foam; ALPORAS

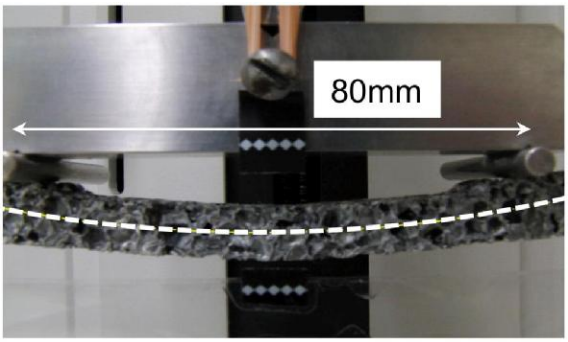

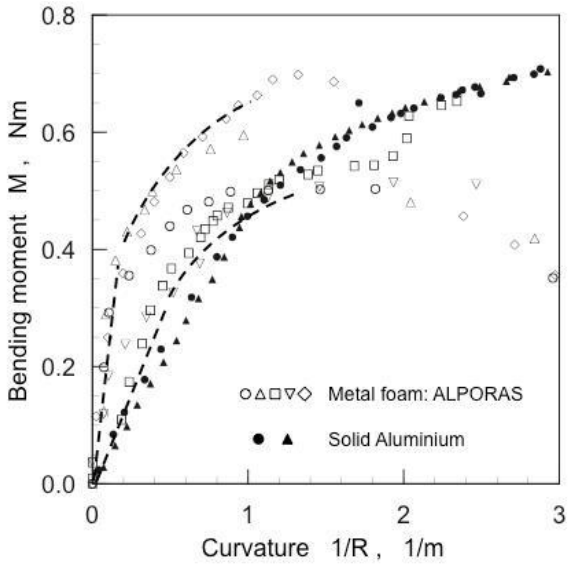

(a) (b)

Figure 2. Four-point bending test. Overview of test specimen (a) and bending-curvature diagrams (b)

3 Material Model

Here we idealize such a real foam as a cellular structure composed of Voronoi polyhedra, and analyze the mechanical response without any periodicity. The model structure is generated with reference to the well-known algorithm, e.g., see Preparata and Shamos (1990), shown in Figure 3 as follows:
(1) A number of species are set at random in three-dimensional space, and each cell boundary is specified as a set of points with equal distance, i.e. a mid-plane, from the corresponding species.
(2) The cell boundary plane is decomposed into triangles, e.g., five triangles for a pentagon in the figure.
(3) Each triangle is again decomposed into three quadrilaterals, setting midpoints of the side of the triangle.
(4) Four-node shell elements are settled to the quadrilaterals, the thickness of which is assumed to be constant over the cell boundary plane.
We notice that this procedure is too idealized compared with the true foam material but this may be a starting point to generate a metal foam model. Further modifications should be made for a more realistic characterization.

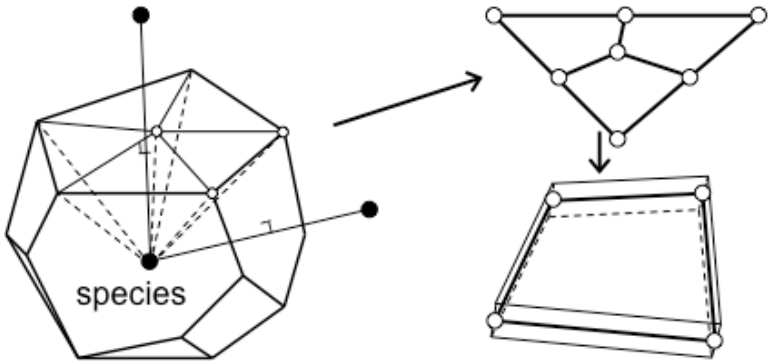

Figure 3. Finite element mesh generation by use of quadrilateral shell element

Three kinds of rectangular cuboid models are generated and used for the finite element analysis. Example meshes are shown in Figure 4 where uniaxial loading at *z*-direction is imposed on the body named "U-model" in Figure 4(a), biaxial loading at *x*- and *y*-directions on "B-model" in Figure (b), and triaxial loading on "T-model" in Figure (c), respectively. A uniform traction or compressive load is hardly achieved because of a variety of shapes in finite element mesh, and so the nodal displacement is prescribed at the end surface of the models. A quasi-uniform deformation is then realized from the macroscopic viewpoint. In order to avoid the end effect, margins with 6 mm are reserved between the end surface boundaries and fictitious internal cuboids, and we concentrate our attention to the macroscopic response of the internal cuboids. We set the dimensions of these internal cuboids (and one cube) as 10x10x20 mm for the U-model, 20x20x10 mm for the B-model, and 10x10x10 mm for the T-model, which are shown in the figure respectively. We confirm that the shape of the internal domain little affects the mechanical response. The number of cells is set as 30 through 120 per unit cube of 1 cm^3, which are relatively coarse, and the porosity as 0.93 with reference to the real metal foam ALPORAS.

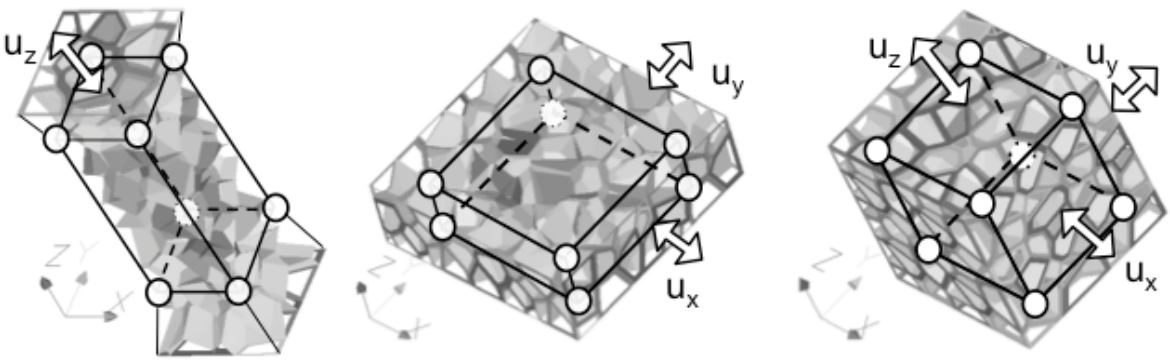

(a) U-model (b) B-model (c) T-model
Figure 4. Three kinds of metal foam models and internal cuboids for the inspection of stress and strain

Forces acting on each surface of the internal cuboids are derived as the sum of corresponding nodal forces, and the stress vector is calculated as the average of force per unit area. Then the stress components are evaluated. This procedure coincides with our empirical concept of stress, although the area of the surface is not infinitesimal but finite in this case. From the numerical test evidence we find that the sums of nodal couples are small enough, i.e. neither twisting nor bending appears at the macroscopic level, and that all the shear stress components are also very small. It follows that we can deal with the normal stress components as the principal stresses. The strain-displacement relation in the finite element procedure is applied to the evaluation of macroscopic strains of the fictitious cuboids. Plural nodes are collected around each corner of the cuboids, and we trace the average movement of the corners. Then the macroscopic strain can be evaluated through the B-matrix technique in the way that the corners are regarded as nodal points. We also define the yield ratio as the volumetric fraction of plastic (yielding) part with respect to the substantial solid volume.

As for the mechanical properties of substantial ingredients, a conventional elastic-plastic model is assumed in the simulation; isotropic linear elasticity and incompressible plasticity with isotropic hardening. We adopt the Young's modulus E = 80 GPa and the Poisson's ration ν = 0.3 for the elasticity, and the initial yield stress σ_y=60 MPa, the hardening coefficient F = 400 MPa and the hardening exponent n = 0.3 for the plasticity, which are typical parameters of soft aluminum alloys. The parameters for the actual metal foam ALPORAS may be different due to the manufacturing process. It is known that the raw material is partly oxidized and that the properties change to those of alumina Al_2O_3. In that case the elasticity modulus should be five or six times larger, and the ductility becomes poor, i.e., F to be larger and n smaller, for the material.

4 Results and Discussions

4.1 Stress-Strain Relation

Macroscopic stress-strain diagrams are shown in Figure 5 where the development of the yield ratio is also depicted in the lower figure. We confirm that the dispersion of the data is not so remarkable as the experimental ones; the variation within 10% in stress response is observed for different mesh patterns. Since we employ the Voronoi tessellation technique in three dimensions, the volumes of the cells are more or less similar. In contrast, the real metal foams involve numerous cells with a variety of volume. Such a discrepancy between the models and the real material causes quantitative differences, and hereafter we discuss the responses for the idealized models.

The shape of all the curves in the figure is similar to that of solid metals; e.g. clear yielding and work-hardening. For the uniaxial stretch, the stress response of the U-model is about 30% lower than that of the T-model, and the elasticity response is also different. The uniaxial stretch in the T-model is carried out in a way that the nodal displacements at x- and y-directions are controlled so as to achieve small stresses σ_x and σ_y, i.e. two or three orders smaller than the σ_z-component. For simple solid materials, these two cases must result in the same response. However, the fact that the sums of the forces are zero in the T-model does not mean the stresses to be free at the x- and y-directions from the local point of view. Some additional constraints are loaded in order to maintain the uniaxial stretch of the cellular foam model. In contrast, all the nodal forces are strictly zero at the x- and y-boundaries in the U-model. It follows that this internal deformation may induce additional stresses in tension and that the response depends both on the loading patterns and on the configuration of the sample cells, even when the macroscopic loading path is the same. If we take the representative volume to be large enough, the results may be asymptotically similar. But such a modelling may not idealize the real sheet properties. In the case of balanced biaxial stretch by the B-model, a slight difference is observed between the σ_x- and σ_y-components, which is a result of anisotropy by the initial cell configuration. The T-model nearly describes a single curve by all the components. Even under the equi-triaxial stretching the model material reveals a clear yielding and subsequent hardening. It means that the model is compressible in plasticity.

The other characteristic feature is observed in the development of the yield ratio, which depends on the loading path and multi-axiality. In the equi-triaxial loading, the onset of plastic yielding occurs everywhere at one time. It suggests that the stress states in each cell, or even in a part of the cells, are almost the same in view of plastic yielding, while the configurations are completely different. In contrast the yield ratio gradually increases in the U-model, and 10% of the skeletal members in the volume do not deform plastically even at ε_z=0.005 (0.5%) when the material clearly reveals a plastic deformation. It tells us that some specific cell members mainly carry the load, and the others do not contribute to the resistance against the external loading under the loading paths deviated from the equi-triaxial loading.

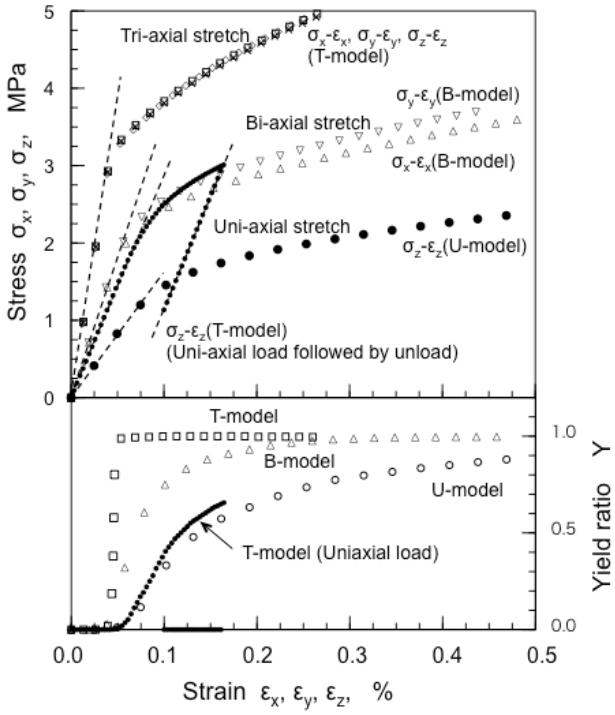

Figure 5. Stress-strain diagram of the model

Figure 6 shows the variation of the macroscopic elasticity modulus E with respect to the number of Voronoi cells in a 10 mm sample cube. The elasticity modulus is derived from the slope of the stress-strain diagram based on the assumption of material isotropy. The modulus of elasticity varies both with the number of cells and the type of material model. When increasing the number of cells in the cuboids or cubes, the elasticity modulus slightly increases, but this tendency is not so remarkable. The elasticity modulus may approach a certain value under a sufficiently large number of cells, although it is contradictive to the real condition in which only a few cells are involved though the thickness. As is also presented in Figure 5, it is characteristic to show the elasticity moduli by the U-model as about 2000 MPa whereas the other ones by the B- and the T-models reveal more than 30% higher, i.e. 2700-3000 MPa. Such results can only be observed in complex materials with internal structures, in which the constraint inside the cells gives dominant influences on the macroscopic response. Compared with the elasticity properties in the experiments, the models predict slightly larger values.

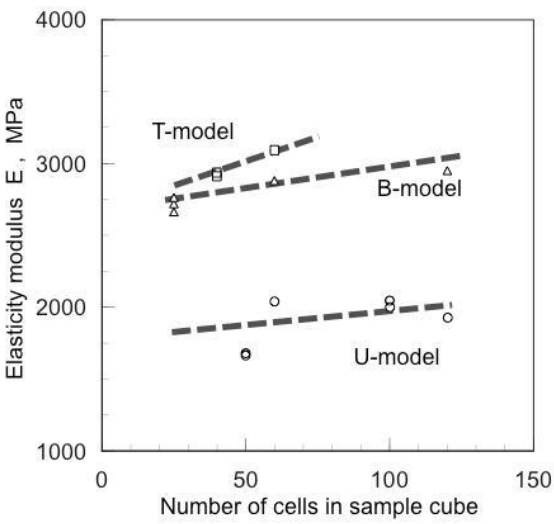

Figure 6. Effect of the number of cells on elasticity modulus

4.2 Yielding and Plastic Flow

We next examine the shape of the yield surface and the normality rule by use of the T-model with 40 cells in the 10 mm sample cube. Various loading paths are imposed on the cubic model with several mesh patterns, so that the yield surface can be specified. Here we do not use the yield stress as the stress level with a certain proof strain but the stress following several levels of yield ratios; e.g., 0.1, 0.3 and 0.5. Figure 7(a) demonstrates the bird-eye-view of yield surface in the three dimensional stress space. The yield ratio is fixed as 0.3 in this Figure where the von Mises yield criterion is described as a cylinder for reference. We find that the material model shows an isotropic response and that the model goes to yielding also under equi-triaxial loading states, i.e. compressible plasticity. This implies that the projection of the yield surface on the π-plane reveals a circle, whereas the yield surface nearly comprises an ellipsoid in the principal stress space. Furthermore, the direction of the plastic strain rate is plotted in the Figure, where the plastic term is derived from subtracting the elastic component from the total strain rate. We can roughly say that the plastic strain rate is generated normal to the yield surface. It follows that we can employ the conventional plasticity concept of associate flow in the macroscopic modelling of foam-like materials. In order to highlight the compressibility of plastic deformation, the yield loci are plotted in detail in Figure 7(b) on the stress plane perpendicular to the π-plane. The incompressibility is also drawn with broken lines in the figure. Three curves are very close at the equi-triaxial stress states of (±3.2, ±3.2, ±3.2), i.e. triaxial tension and compression (pressure), and there we observe a sudden change from elasticity to plasticity. In contrast, the plastic yielding gradually makes progress under the uniaxial stress states from 1.8 MPa to 2.5 MPa or under combined stress states of tension and compression including shear loading. The normality rule roughly holds in any stress state. However, we have to notice that the plastic strain rate includes the variation of elastic strain, except for the equi-triaxial case, because the yield ratio evolves during the loading, and some cell members deforms elastically.

We finally evaluate the yield condition for a plate-like material model B, the configuration of which is more similar to the actual metal foam supplied, and compare the yield locus with the results by the T-model and the U-model. The number of cells in a 10mm sample cube is set 30 through 60, which does not affect the variation in yield stress. Figure 8 shows the comparison of yield surface in plane stress condition, in which the yield loci by the B-model is drawn in solid lines and those by the T-model in broken lines. The von Mises type isotropic yield loci are also shown in dotted lines for convention. The yield stresses by the B-model are located between those by the U-model and the T-model. Such a difference arises from the influence of the free surface boundary. Lack of constraint at *z*-direction by the B-model reduces the stresses inside the sample cube or cuboid, and this appears as the yielding at stress levels lower than those by the T-model. It should be noted that a significant anisotropy appears at the yield ratio of 0.5 by the B-model in the way that the stress levels under uniaxial loading and shear loading are similar to those of the U-model whereas the material yields at higher stress levels under balanced equi-biaxial loading, i.e. more distorted shape of ellipse is found at that direction. In order to formulate a practical constitutive model for such cellular materials with finite dimension in the thickness, we have to take account of the anisotropy arising from the configuration of targeted material. This kind of anisotropy significantly appears following the shape whether it is prepared as plates or bars.

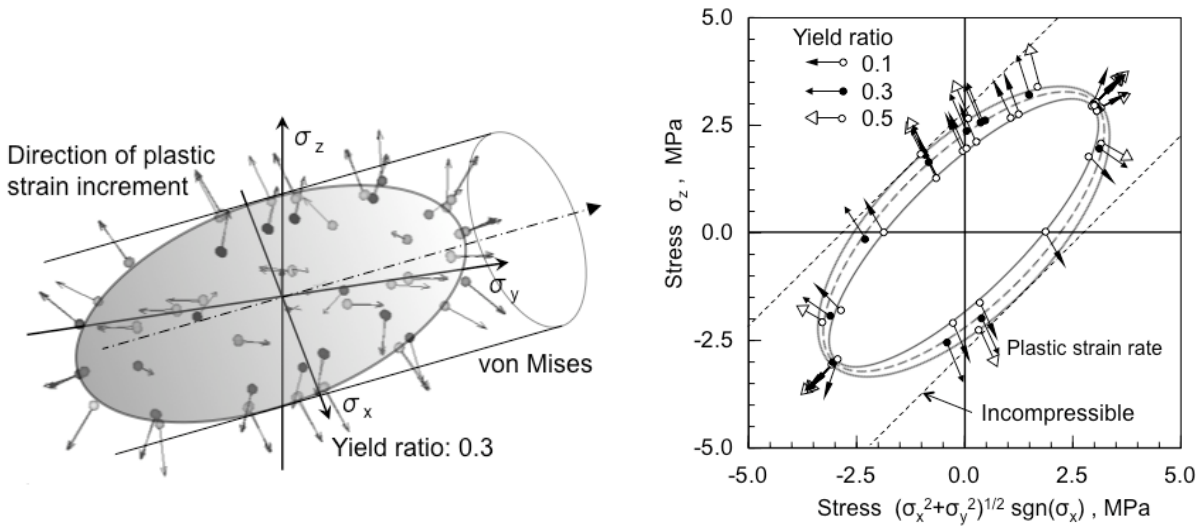

(a) Over view (b) Compressibility

Figure 7. Yield surface and plastic flow in stress space

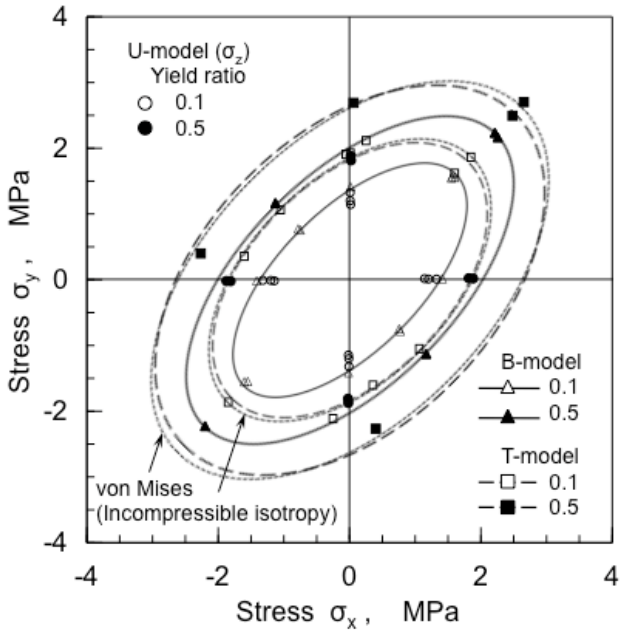

Figure 8. Comparison of yield loci in plane stress condition

5 Concluding Remarks

In order to evaluate the macroscopic response of metal foam, a numerical study is carried out on model materials with cellular structure. Closed cell models are constructed by use of computational technique of the Voronoi tessellation and applied to the finite element analysis. We notice that the models employed in the simulation are too simply idealized and that further analyses should be carried out for evaluating the porosity dependence, the morphology dependence and the imperfection effects. However, we expect that the essence of the deformation mechanism can be captured at the macroscopic level. We focus our attention to a practical situation where a relatively small amount of cells are located in the domain, particularly in the thickness direction, and the transition from elasticity to plasticity is discussed. We found the following results through the simulations:
(1) Similar stress-strain response to solid metals can be found at the beginning of the plastic deformation in view of clear yielding and work-hardening. As a matter of course the material is compressible in plasticity regime.
(2) The mechanism of macroscopic yielding depends on the loading pattern or deformation mode; all the cells fall into yielding at one time under equi-triaxial loading whereas yielding gradually makes progress under uniaxial loading. A part of the cells remains elastic under the uniaxial loading even when the material reveals a macroscopic yielding at the strain level of 0.005.
(3) The elasticity modulus depends on the configuration of the sample structures; the elastic properties change whether the material is composed of bars, plates or brick so far as the number of cells is small in the objective sample. This is due to the constraint by the surrounding and also gives influence on the macroscopic anisotropy.
(4) The yield surface reveals an ellipsoid in the principal stress space and the normality rule holds also from the macroscopic view. It implies that we can adopt the conventional plasticity concept in formulating a constitutive model.
(5) A significant anisotropy is observed in a plate-like material model because of the internal constraint. When dealing with a metal foam plate, it is of importance to take account of this anisotropy in the thickness direction because lower stresses are found in uniaxial state including in-plane shear. It is not sure, however, whether we can deal with this anisotropy within the simple material concept.

Acknowledgments
A part of the work is supported by the Japan Society of Promotion of Science (JSPS) as a Grant-in-Aid for Scientific Research (No. 22560080). The author thanks Mr. R. Nakano for conducting the experiments and Dr. M. Kanemaru of SHINKO Wire Co LTD for providing the test material.

References

Ashby, M. F.; Evans, A.; Fleck, N. A.; Gibson, L. J.; Hutchinson, J. W.; Wadley, H. N. G.: *Metal Foams: A Design Guide*. Butterworth Heinemann, UK (2000).

Belytschko, T.; Leviathan, I.: Physical stabilization of the 4-node shell element with one point quadrature. *Comp. Methods Appl. Mech. Engrg.*, 113, (1994), 321-350.

Deshpande, V. S.; Fleck, N. A.: Isotropic constitutive models for metallic foams. *J. Mech. Phys. Solids*, 48, (2000), 1253-1283.

Diebels, S.; Steeb, H.: The size effect in foams and its theoretical and numerical investigation, *Proc. R. Soc. Lond.* A, 458, (2002), 2869-2883.

Dillard, T.; Forest, S.; Ienny, P.: Micromorphic continuum modelling of the deformation and fracture behaviour of nickel foams. *Euro. J. Mech. A/Solids*, 25, (2006), 526-549.

Preparata, F. P.; Shamos, M. I.: Computational Geometry: An Introduction. Springer-Verlag, Germany (1990).

Tekoglu, C. Gibson, L. J.; Pardoen, T; Onck, P. R. Size effects in foams: Experiments and modelling, *Prog. Mater. Sci.*, 56, (2011), 109-138.

Zhu, Y; Zacharia, T: A new one-point quadrature, quadrilateral shell element with drilling degrees of freedom. *Comp. Methods Appl. Mech. Engrg.*, 136, (1996), 165-203.

Address: Assoc. Prof. Shoji Imatani, Department of Energy Conversion Science, Kyoto University, 6068501 Kyoto, Japan, email: imatani@energy.kyoto-u.ac.jp